CHINESE OPTICS LETTERS

Vol. 19, No. 7 | July 2021

In-situ modal inspection based on transverse second harmonic generation in single CdS nanobelt

Chenguang Xin (辛晨光)[1,2,3*], Jie Qi (亓 杰)[1,2], Rui Zhang (张 瑞)[1,2], Li Jin (金 丽)[1,2], and Yanru Zhou (周彦汝)[4**]

[1] Academy for Advanced Interdisciplinary Research, North University of China, Taiyuan 030051, China

[2] School of Instrument and Electronics, North University of China, Taiyuan 030051, China

[3] State Key Laboratory of Modern Optical Instrumentation, College of Optical Science and Engineering, Zhejiang University, Hangzhou 310027, China

[4] School of Information and Communication Engineering, North University of China, Taiyuan 030051, China

*Corresponding author: xincg@nuc.edu.cn

**Corresponding author: zhouyanru@nuc.edu.cn

Received August 31, 2020 | Accepted December 5, 2020 | Posted Online March 16, 2021

Based on the transverse second-harmonic generation (TSHG) effect, we demonstrate a method for *in-situ* modal inspection of nonlinear micro/nanowaveguides. Pumping lights are equally split and coupled into two ends of a single CdS nanobelt (NB). As pumping light counter-propagates along the NB, transverse second-harmonic (TSH) interference patterns are observed. The influence of multimode interaction on the TSHG effect is discussed in detail. Using fast Fourier transform, TSH interference patterns are analyzed, indicating the existence of at least four modes inside the NB. Experimental beat lengths are found to be in agreement with calculated results.

Keywords: micro/nanowaveguides; transverse second-harmonic generation; multimode interference; modal inspection.
DOI: 10.3788/COL202119.071901

1. Introduction

Highly confined optical modes in micro/nanowaveguides have broad applications spanning from atomic systems, particle trapping, high-bit-rate optical communication to optical sensing[1–10]. So far, a variety of techniques have been developed for modal inspection of micro/nanowaveguides. One common method is direct imaging of modal profiles at the output end[11]. However, the method is not applicable for the presentation of the mode evolution process. Another approach is using near-field scanning optical microscopy (NSOM) to detect the evanescent field[12–14]. For the method, complex operating systems are generally required. Modal inspection based on Rayleigh scattering has also been reported, which is limited by a rather weak signal collection from geometrically uniform fibers[15,16]. Recently, direct observation of multimode interference in rare-earth-doped micro/nanofibers has been demonstrated[16]. However, since the approach is based on up-conversion luminescent interference, it is still challenging to observe multimode interference directly in passive micro/nanowaveguides.

Benefitting from attractive features such as high scalability and compatibility, transverse second-harmonic generation (TSHG) and transverse third harmonic generation (TTHG) in optical waveguides have been attracting continuous attentions for developing integrated photonic circuits and devices[17–21]. In 2016, an optical correlator was reported based on the TSHG effect in a single CdTe nanowire[22]. Benefitting from high nonlinearity, the input energy went down to a fJ/pulse level.

In this paper, we demonstrate *in-situ* modal inspection based on the TSHG effect inside a single CdS nanobelt (NB). With 1064 nm pumping light coupled in, transverse second-harmonic (TSH) interference patterns are observed in the direction perpendicular to axis of the NB. Modal superposition is analyzed using the fast Fourier transform (FFT) method. A few modes, including fundamental mode and several high-order modes, are extracted from FFT results of the TSH interference patterns, which are in agreement with calculated results. With the assistance of the refractive index difference (Δn_{eff}) between different optical modes, we have also investigated the period of TSH patterns in theory, revealing the characteristic of modal dispersion. It is worth mentioning that this method can be, in principle, operated for many varieties of nonlinear micro/nanowaveguides (e.g., ZnO, CdS, CdTe, GaAs, $LiNbO_3$)[23–25].

2. Experiment

The CdS NBs with widths ranging from a few to a couple of micrometers and a height of a few hundred nanometers were synthesized by a thermal evaporation process[26,27]. Electron and optical microscope characterizations confirm a uniform

dimension and smooth surface, as shown in Fig. 1, indicating a rather low optical propagating loss[28].

The experiment setup is schematically illustrated in Fig. 2. A CdS NB is placed across a slit of two MgF_2 substrates. The continuous wave (CW) pumping light is split into two parts equally and coupled into the NB from both ends using fiber tapers. As counter-propagating light overlaps with each other in the NB, the TSH signal can be collected in the direction perpendicular to the axis of the NB using an object lens, as required by the wave-vector matching condition[18,19].

Supposing that, there are two counter-propagating modes with propagating constants of β_ω and β'_ω, respectively, inside the NB, as shown in Fig. 3. Determined by the phase matching condition, the emitting angle (θ) of TSH light is given by

$$\cos\theta = \left|\frac{\beta_\omega - \beta'_\omega}{k_{2\omega}}\right|, \tag{1}$$

where $k_{2\omega}$ is the wave vector of TSH light. Since the propagating constants for different optical modes at the same wavelength differ with each other, θ is slightly different from 90° for the TSHG process involving different modes.

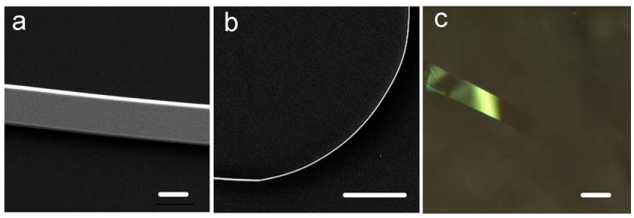

Fig. 1. CdS NBs. (a) Scanning electron microscope image of upper face (scar bar, 1 μm). (b) Scanning electron microscope image of side face (scar bar, 5 μm). (c) Optical microscope image (scar bar, 10 μm).

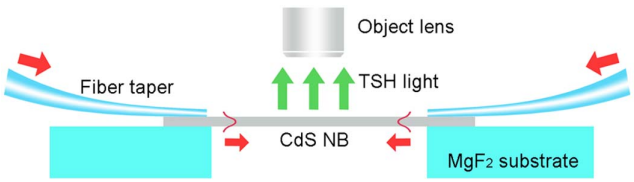

Fig. 2. Schematic diagram of the experiment. CdS NB is placed across a slit of two MgF_2 to avoid influence from substrates.

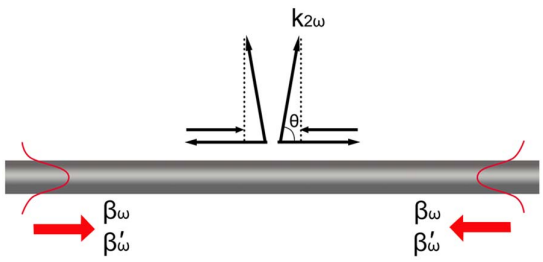

Fig. 3. Emitting angle determined by the phase matching condition.

Multimode interference also results in periodic TSH interference patterns along the axis of the NB. The period (D) can be expressed by[29]

$$D = \frac{\pi}{|\beta_\omega - \beta'_\omega|}. \tag{2}$$

Although the phase matching condition is not applied in the direction perpendicular to the axis of the NB, the obvious TSHG effect is also expected. For TSHG in a single micro/nanowaveguide, a coherent length caused by phase mismatch in the direction perpendicular to the axis of the waveguide can be estimated as[30]

$$L_c = \frac{\pi}{\Delta k}. \tag{3}$$

The phase mismatch is given by

$$\Delta k = k_{2\omega} \bullet \cos\theta = \frac{2\pi n_{2\omega}}{\lambda_{2\omega}} \bullet \cos\theta, \tag{4}$$

where $n_{2\omega}$ and $\lambda_{2\omega}$ are the refractive index and vacuum wavelength of TSH light, respectively. Considering a simplified case in which the TSHG effect is only caused by counter-propagating modes with the same propagating constant, θ should be 90° according to Eq. (1), and L_c can be described by

$$L_c = \frac{\lambda_{2\omega}}{2n_{2\omega}}. \tag{5}$$

For CdS NBs, we obtained an L_c of ~102 nm at a pumping wavelength of 1064 nm. Therefore, a relatively strong TSH signal is expected for CdS NBs with a height of a few hundred nanometers[22,29].

To demonstrate the TSHG effect experimentally, a CdS NB with a width of 2 μm and a height of 200 nm was used [Fig. 4(a)]. As 1064 nm pumping light with a power of 5 mW is coupled in, green TSH light was observed. As shown in Fig. 4(b), there were obvious luminescent patterns with a period of ~9.3 μm along the axis of the NB, which is believed to be owing to optical interference caused by multimode interaction. The mode profiles and effective refractive index were analyzed by finite-difference time-domain (FDTD) simulation. For the fundamental mode, power is concentrated on the center of the NB. However, for the second-order mode, power falls into two parts, which is distributed symmetrically along the axis. Considering the calculated effective refractive indices of 1.868 and 1.812 for the fundamental mode and the second-order mode, respectively, the period of TSH patterns can be calculated to be ~9.5 μm, agreeing well with the experimental result (~9.3 μm). The emitting angle was calculated to be ~88.4° using Eq. (1).

To demonstrate the influence of multimode interference on luminescent patterns, the TSH signal in a single nanowire with

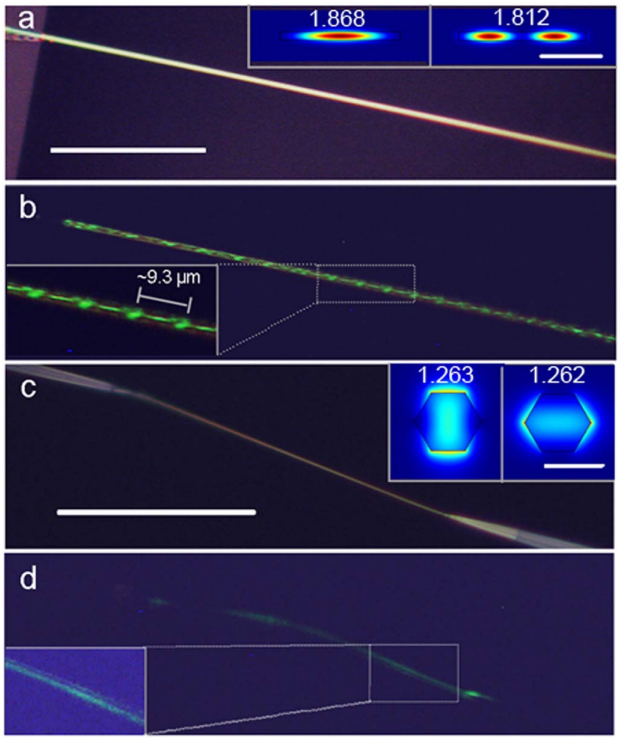

Fig. 4. (a) Optical microscope image of a 2-μm-wide CdS NB with a height of 200 ± 10 nm (scar bar, 50 μm). Inset shows simulated profiles of the fundamental and second-order modes inside an NB at a wavelength of 1064 nm (scar bar, 1 μm). In the FDTD simulation, the width is 2 μm, and the height is 200 nm. (b) TSH interference patterns for the CdS NB with 1064 nm CW light input. (c) Optical microscope image of a 300 nm diameter nanowire (scar bar, 50 μm). Inset shows simulated profile of the first and second-order modes at a wavelength of 1064 nm (scar bar, 300 nm). In the simulation, the nanowire has a hexagonal cross section, which agrees with the reality. The side-to-side diameter is 300 nm. (d) TSH patterns for the nanowire with 1064 nm CW light input.

a diameter of 300 ± 10 nm was also collected [Fig. 4(c)]. Considering a much smaller dimension, the effective refractive index for modes inside the nanowire is much smaller. As a result of better symmetry for the cross section, the effective refractive index difference between the fundamental mode and the second-order mode inside the nanowire is also much smaller than that in an NB. There was no obvious period observed within a length of ~100 μm, as shown in Fig. 4(d). It is reasonable, considering a calculated interference period over 500 μm is extracted from a rather small Δn_{eff} of ~0.001 between the fundamental mode and the second-order mode inside the nanowire.

The green signal was analyzed by a spectrometer (iHR550, HORIBA Inc.) after passing through a 1064 nm blocking notch filter (Edmund, Inc.). As shown in Fig. 5(a), within a broad spectral range, there are no other peaks except for two peaks corresponding to the pumping light at 1064 nm and the TSH light at 532 nm. The TSH signal intensity with different input power is shown in Fig. 5(b), confirming a second-order nonlinear relationship.

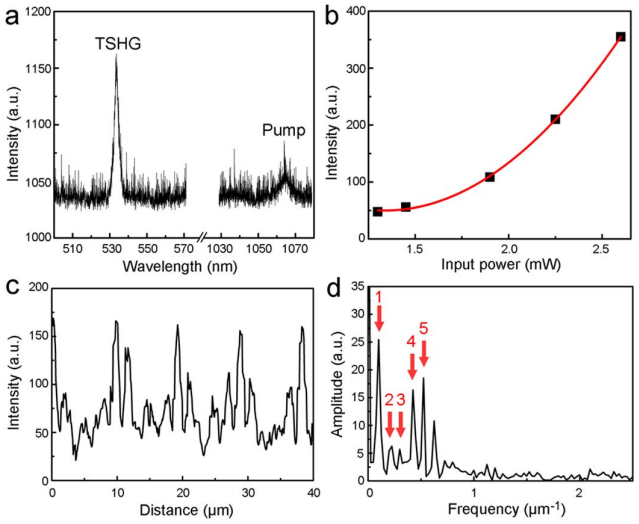

Fig. 5. (a) Measured spectrum of TSH signal. (b) Intensity of the TSH signal with different input power. (c) Extracted intensity profile for the TSH signal along the axis of the NB, corresponding to the inside image of Fig. 4(b). (d) Corresponding FFT spectrum. The arrows indicate the first five peaks in the spectrum.

3. Discussion

To analyze the TSH patterns, we extracted the image intensity along the axis of the NB in the inside image of Fig. 4(b). The intensity profile is shown in Fig. 5(c), indicating an obviously strong oscillation. The corresponding FFT spectrum was obtained, as shown in Fig. 5(d). The red arrows show the first peaks located at 0.100 μm^{-1}, 0.225 μm^{-1}, 0.299 μm^{-1}, 0.424 μm^{-1}, and 0.524 μm^{-1}, respectively. Considering a resolution of ~0.025 μm^{-1} [16], the results are in good agreement with calculated values (0.105 μm^{-1}, 0.181 μm^{-1}, 0.286 μm^{-1},

Table 1. Comparison between Calculated Results of Modal Interference and Experimental Results[a].

No.	Modes	Δn_{eff}	Period (μm)	Calculated Frequency (μm^{-1})	Experimental Data (μm^{-1})
1	1st & 2nd	0.0556	9.53	0.105	0.100
2	2nd & 3rd	0.0960	5.52	0.181	0.225
3	1st & 3rd	0.1516	3.49	0.286	0.299
4	2nd & 4th	0.2385	2.22	0.450	0.424
5	1st & 4th	0.2942	1.80	0.555	0.524

[a]The height of the NB used in the simulation is 200 nm.

0.450 μm^{-1}, and 0.555 μm^{-1}, respectively), as shown in Table 1. The calculated results are obtained with a width of 2 μm and a height of 200 nm. The results demonstrate the existence of at least four modes inside the NB. For example, the first peak located at 0.100 μm^{-1} is supposed to arise from optical interference between the fundamental mode and the second-order mode, corresponding to a calculated frequency of 0.105 μm^{-1}.

Considering a 20 nm resolution of the scanning electron microscope image, we have also calculated modal interference with different heights. With heights ranging from 190 nm to 210 nm, the calculated results are very similar (as shown in Table 2). The results show that a change of 20 nm in height does not introduce significant difference into modal interference inside the NB.

The influence of the surrounding refractive index on TSH patterns is discussed. According to Eq. (2), D is inversely related to Δn_{eff} (the effective refractive index difference between the fundamental mode and the second-order mode). As the surrounding refractive index increases, the effective refractive index of both the fundamental mode and the second-order mode increases, as shown in Fig. 6. A downward trend of Δn_{eff} between the two modes with an increasing surrounding refractive index is also obtained. It is reasonable to consider a less optical confinement, which means more fields are spreading into the surrounding area from the NB, for higher-order modes[31,32].

Table 2. Calculated Results of Modal Interference with Different Heights of NBs.

		Modal Interference (μm^{-1})		
No.	Modes	190 nm	200 nm	210 nm
1	1st & 2nd	0.106	0.105	0.104
2	2nd & 3rd	0.183	0.181	0.179
3	1st & 3rd	0.289	0.286	0.283
4	2nd & 4th	0.455	0.450	0.445
5	1st & 4th	0.562	0.555	0.549

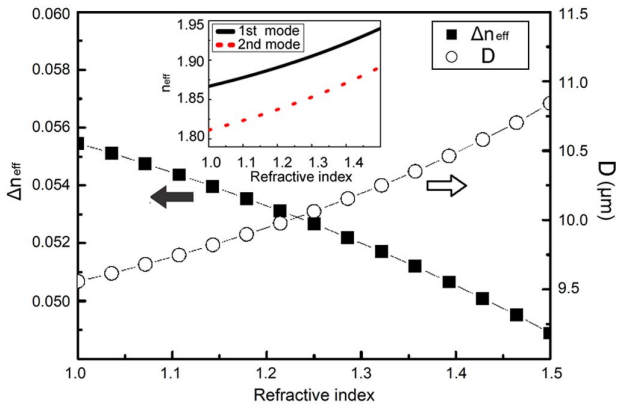

Fig. 6. Δn_{eff} and D with different surrounding refractive indices. Inside image shows calculated effective index for the fundamental mode and the second-order mode, respectively. The width of the NB is 2 μm.The height of the NB is 200 nm. The pumping wavelength is 1064 nm.

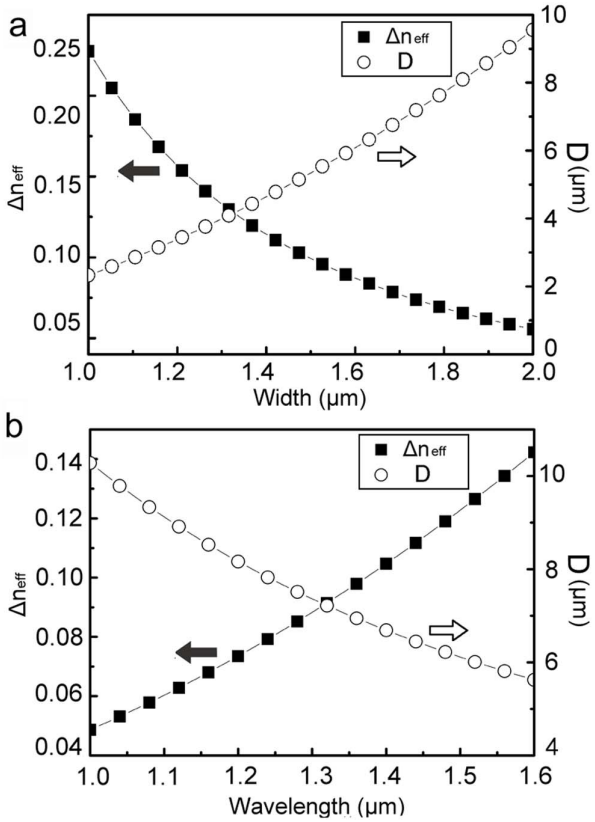

Fig. 7. (a) Δn_{eff} and D with different widths of NBs. The pumping wavelength is 1064 nm. (b) Δn_{eff} and D at different wavelengths for a 2-μm-wide CdS NB. The height of the NB is 200 nm.

Similarly, the relationship between D and the waveguide dimension is also investigated by FDTD simulation, as shown in Fig. 7(a). For example, as the width of the CdS NB increases from 1.0 to 2.0 μm, Δn_{eff} changes from ~0.25 to ~0.05, leading to a ~ 5 times larger D for TSH patterns.

Δn_{eff} with a different wavelength is also discussed to reveal the characteristic of modal dispersions theoretically, as shown in Fig. 7(b). For a larger pumping wavelength, there is a greater Δn_{eff}. Combining the fact that both modes have negative dispersions within the near-infrared spectral range, we can deduce that the fundamental mode has a smaller absolute dispersion than the second-order mode.

4. Conclusion

In conclusion, we demonstrate *in-situ* modal inspection based on direct observation of TSH interference patterns from a single nonlinear CdS NB. Benefitting from subwavelength-scale sectional dimension of the NB, a strong TSH signal is observed.

Using the FFT method, TSH interference patterns are analyzed. The experimental results agree well with the calculated results, demonstrating the existence of at least four modes inside the NB. The influence of multimode interference on the TSHG effect inside a single micro/nanowaveguide is discussed in detail. The relationships among the period of TSH patterns, the surrounding refractive index, waveguide dimension, and pumping wavelength are also investigated, respectively, revealing dispersion properties for optical modes. Based on the wavelength conversion process, *in-situ* modal inspection of infrared propagating light has been demonstrated using a visible imaging system. Since the mechanism for transverse interference patterns can also be other nonlinear processes such as TTHG, the method can be, in principle, operated in micro/nanowaveguides with either second-order nonlinearity or third-order nonlinearity, which may find applications on multimode nanophotonic devices such as optical sensors and correlators.

Acknowledgement

This work was supported by the Scientific and Technologial Innovation Programs of Higher Education Institutions in Shanxi (No. 2019L0587-19004454).

References

1. E. Li, X. Wang, and C. Zhang, "Fiber-optic temperature sensor based on interference of selective higher-order modes," Appl. Phys. Lett. **89**, 091119 (2006).
2. L. Li, Q. Lou, J. Zhou, J. Dong, Y. Wei, and J. Li, "High power low-order modes operation of a multimode fiber laser," Chin. Opt. Lett. **5**, 221 (2007).
3. N. Bozinovic, Y. Yue, Y. Ren, M. Tur, P. Kristensen, H. Huang, A. E. Willner, and S. Ramachandran, "Terabit-scale orbital angular momentum mode division multiplexing in fibers," Science **340**, 1545 (2013).
4. G. Labroille, B. Denolle, P. Jian, P. Genevaux, N. Treps, and J.-F. Morizur, "Efficient and mode selective spatial mode multiplexer based on multi-plane light conversion," Opt. Express **22**, 15599 (2014).
5. J. E. Hoffman, F. K. Fatemi, G. Beadie, S. L. Rolston, and L. A. Orozco, "Rayleigh scattering in an optical nanofiber as a probe of higher-order mode propagation," Optica **2**, 416 (2015).
6. V. G. T. A. Maimaiti, M. Sergides, I. Gusachenko, and S. N. Chormaic, "Higher order microfiber modes for dielectric particle trapping and propulsion," Sci. Rep. **5**, 9077 (2015).
7. X. Zhang, R. Chen, Y. Zhou, H. Ming, and A. Wang, "Mode selective coupler for optical vortices generation," Chin. Opt. Lett. **15**, 030008 (2017).
8. Y. Huang, F. Shi, T. Wang, X. Liu, X. Zeng, F. Pang, T. Wang, and P. Zhou, "High-order mode Yb-doped fiber lasers based on mode-selective couplers," Opt. Express **26**, 19171 (2018).
9. Q. Yuan, L. Fang, Q. Zhao, Y. Wang, B. Mao, V. Khayrudinov, H. Lipsanen, Z. Sun, J. Zhao, and X. Gan, "Mode couplings of a semiconductor nanowire scanning across a photonic crystal nanocavity," Chin. Opt. Lett. **17**, 062301 (2019).
10. Z. Song, X. Yue, Y. Luo, H. Li, and Y. Zhao, "Absorption saturation measurement using the tapered optical nanofiber in a hot cesium vapor," Chin. Opt. Lett. **17**, 031901 (2019).
11. Y. Zhang, H. Li, C. Dai, L. Xu, C. Gu, W. Chen, Y. Zhu, P. Yao, and Q. Zhan, "All-fiber high-order mode laser using a metal-clad transverse mode filter," Opt. Express **26**, 29679 (2018).
12. K. Foubert, L. Lalouat, B. Cluzel, E. Picard, D. Peyrade, E. Delamadeleine, F. de Fornel, and E. Hadji, "Near-field modal microscopy of subwavelength light confinement in multimode silicon slot waveguides," Appl. Phys. Lett. **93**, 251103 (2008).
13. F. Gesuele, C. X. Pang, G. Leblond, S. Blaize, A. Bruyant, P. Royer, R. Deturche, P. Maddalena, and G. Lerondel, "Towards routine near-field optical characterization of silicon-based photonic structures: an optical mode analysis in integrated waveguides by transmission AFM-based SNOM," Physica E **41**, 1130 (2009).
14. J. I. Ziegler, M. W. Pruessner, B. S. Simpkins, D. A. Kozak, D. Park, F. K. Fatemi, and T. H. Stievater, "3-D near-field imaging of guided modes in nanophotonic waveguides," Nanophotonics **6**, 1141 (2017).
15. G. P. Agrawal, *Fiber-Optic Communication Systems* (Wiley, 2010).
16. B. Chen, Q. Bao, and L. Tong, "Direct observation of multimode interference in rare-earth doped micro/nanofibers," Opt. Express **27**, 26728 (2019).
17. R. Normandin and G. I. Stegeman, "Picosecond signal processing with planar, nonlinear integrated optics," Appl. Phys. Lett. **36**, 253 (1980).
18. R. Fischer, D. N. Neshev, S. M. Saltiel, A. A. Sukhorukov, W. Krolikowski, and Y. S. Kivshar, "Monitoring ultrashort pulses by transverse frequency doubling of counterpropagating pulses in random media," Appl. Phys. Lett. **91**, 031104 (2007).
19. C. Monat, C. Grillet, M. Collins, A. Clark, J. Schroeder, C. Xiong, J. Li, L. O'Faolain, T. F. Krauss, B. J. Eggleton, and D. J. Moss, "Integrated optical auto-correlator based on third-harmonic generation in a silicon photonic crystal waveguide," Nat. Commun. **5**, 3246 (2014).
20. H. Yu, W. Fang, X. Wu, X. Lin, L. Tong, W. Liu, A. Wang, and Y. R. Shen, "Single nanowire optical correlator," Nano. Lett. **14**, 3487 (2014).
21. F. Gu, L. Zhang, G. Wu, Y. Zhu, and H. Zeng, "Sub-bandgap transverse frequency conversion in semiconductor nano-waveguides," Nanoscale **6**, 12371 (2014).
22. C. Xin, S. Yu, Q. Bao, X. Wu, B. Chen, Y. Wang, Y. Xu, Z. Yang, and L. Tong, "Single CdTe nanowire optical correlator for femtojoule pulses," Nano. Lett. **16**, 4807 (2016).
23. S. K. Kurtz and T. T. Perry, "A powder technique for the evaluation of nonlinear optical materials," J. Appl. Phys. **39**, 3798 (1968).
24. I. Shoji, T. Kondo, A. Kitamoto, M. Shirane, and R. Ito, "Absolute scale of second-order nonlinear-optical coefficients," J. Opt. Soc. Am. B. **14**, 2268 (1997).
25. X. Huang, S. Dai, P. Xu, Y. Wang, Q. Yang, Y. Zhang, and M. Xiao, "Resonant and nonresonant second-harmonic generation in a single cadmium sulfide nanowire," Chin. Opt. Lett. **15**, 061901 (2017).
26. A. M. Morales and C. M. Lieber, "A laser ablation method for the synthesis of crystalline semiconductor nanowires," Science **279**, 208 (1998).
27. S. Kar and S. Chaudhuri, "Cadmium sulfide one-dimensional nanostructures: synthesis, characterization and application," Synth. React. Inorg. M. **36**, 289 (2006).
28. C. Xin, H. Wu, Y. Xie, S. Yu, N. Zhou, Z. Shi, X. Guo, and L. Tong, "CdTe microwires as mid-infrared optical waveguides," Opt. Express **26**, 10944 (2018).
29. D. Vakhshoori and S. Wang, "Integrable semiconductor optical correlator, parametric spectrometer for communication systems," J. Lightwave Technol. **9**, 906 (1991).
30. R. W. Boyd, *Nonlinear Optics* (Academic Press, 1992).
31. X. Guo, Y. Ying, and L. Tong, "Photonic nanowires: from subwavelength waveguides to optical sensors," Accounts Chem. Res. **47**, 656 (2014).
32. X. Wu and L. Tong, "Optical microfibers and nanofibers," Nanophotonics **2**, 407 (2013).